Mathematical Geology, Vol. 28, No. 2, 1996

Determination and Interpretation of Preferred Orientation with Texture Goniometry: An Application of Indicators to Maximum Entropy Pole- to Orientation-Density Inversion[1]

H. Schaeben[2] and H. Siemes[2]

The probability density function of orientations of crystals generally cannot be measured directly without destruction of the specimen. Therefore it is usual practice to sample pole density functions of several crystal forms in diffraction experiments with a texture goniometer. Determining a reasonable orientation density function from experimental pole density functions is then the crucial prerequisite of quantitative texture analysis. This mathematical problem may be addressed as a tomographic inversion problem specified by the crystal and statistical specimen symmetries and the properties of the diffraction experiment. Its solution with maximum entropy preferred orientation portion and maximum uniform portion is proposed because it yields the most conservative orientation density function with systematically reduced correlation effects, thus avoiding artificial texture "ghost" components caused by the specific properties of the diffraction experiment.

KEY WORDS: preferred crystal orientation, texture goniometry, quantitative texture analysis, inversion of diffraction pole density functions, entropy optimization, quartzite fabric.

INTRODUCTION

Anisotropic behavior of single phase polycrystalline material is controlled by its constituent crystal grains and their spatial orientation within the specimen. Thus, the statistical distribution of crystal orientations is a simple mathematical approach of describing and quantifying anisotropy.

The orientation-density function generally cannot be measured directly without destruction of the specimen. Therefore it is usual practice to sample pole-density functions of several distinct reflections in X-ray or neutron diffraction experiments with a texture goniometer. Determining a reasonable orientation-density function from experimental pole-density functions then is the crucial prerequisite of quantitative texture analysis. This mathematical problem of tex-

[1]Received 13 March 1994; accepted 18 February 1995.

[2]Department of Mineralogy, University of Technology Aachen, Templergraben 55, 52056 Aachen, Germany.

0882-8121/96/0200-0169$09.50/1

ture goniometry is an inverse projection problem because the measured pole-density functions represent mean orientation densities of the specimen along given lines of integration in some orientation space; it also may be addressed as a tomographic inversion problem specified by the crystal and statistical specimen symmetries and the properties of the diffraction experiment itself. Mathematically it reads as a Fredholm integral equation of first type.

The inversion problem of texture goniometry was tackled conventionally by transform methods, that is harmonic series expansions. Because of the specifics of the problem these methods are unable to recover the part of the orientation-density function represented by the odd terms of the harmonic series expansion. In this situation, discrete methods have been developed primarily because they are capable of incorporating additional information, especially the nonnegativity of the orientation-density function to be determined, as truly constitutive elements of an inversion procedure. The discrete approach leads to a system of linear equations which is large, sparse, structureless, highly (column)rank deficient, and may be inconsistent.

Its solution with maximum entropy preferred orientation portion and maximum uniform portion is proposed because it yields the nonnegative orientation-density function as close (with respect to entropy) to the uniform probability density as possible subject to its being consistent with the given experimental pole-density function data, that is the orientation-density function with systematically reduced correlation effects, thus avoiding artificial texture "ghost" components caused by the specific properties of the diffraction experiment. Mathematically, the maximum entropy solution is characterized as the particular one around which all solutions are concentrated. The principle of maximum entropy has been referred to as "principle of maximum objectivity," "principle of minimum bias," "principle of minimum prejudice," "principle of maximum honesty," etc. (cf. Kapur, 1983).

The discrete approach also provides the option to determine an upper and lower bound for the orientation density of each texture component resulting in a numerical "confidence interval" for each individual component and eventually in a "variation width" of the entire set of feasible orientation-density functions. Yet another option is that the initial system of linear equations can be replaced by a system of inequalities if measurement errors are supposedly large and have to be taken into account explicitly.

In comparison with the harmonic method the major advantages of the discrete approach may be summarized that entropy optimization results in the most conservative feasible orientation density function and that further confidence intervals or variation width aid in a safe, that is conservative interpretation. In view of the fact that orientation-density functions calculated from pole-density functions depend to a large extent on additional heuristic or mathematical mod-

eling assumptions involved to specify it, confidence intervals and variation width may prove most substantial when the initial "real world" problem itself is an inverse one like reconstructing the geological deformation history from observed patterns of preferred orientations in rocks.

Mathematical Description of Macroscopic Anisotropy by the Orientation-Density Function

Materials with polycrystalline structure are composed of crystallites of various size, shape, and crystallographic orientation. Each crystal's orientation (denoted g) can be defined with respect to external coordinates by a rotation, that is, by three angles. Orientations of crystals can be determined with optical, electron or X-ray diffraction, and other techniques. Orientations within a specimen of a polycrystalline material may be described summarily with an orientation distribution which can be uniform or display preferred orientation. If the orientation distribution of the crystals is not uniform, the material generally will be anisotropic because of the anisotropy of crystal properties. Macroscopic anisotropy thus is a fundamental property of all polycrystalline materials.

Based on the orientation-density function as a constitutive variable of the polycrystalline state of matter, model calculations of physical properties as well as of texture development have attained increasing interest. This applies to virtually all types of anisotropic physical properties such as elastic, plastic, electric, magnetic, thermal, optical, and chemical properties as well as to various types of solid state processes such as primary crystallization, plastic deformation, recrystallization, or phase transformation.

The determination and interpretation of preferred orientation of crystals in deformed polycrystalline aggregates—here referred to as texture analysis—has been of longstanding concern to both material scientists and geologists (Wenk, 1985; Wenk and others, 1988).

Texture Analysis in Geosciences

The major objectives of texture analysis in metallurgy and in geosciences, however, are different not only with respect to the investigated materials.

In metallurgy, it typically addresses problems such as what pattern of preferred crystal orientation is caused by a given process, and refers to process control in the laboratory or quality control in production to guarantee a required preferred crystal orientation and corresponding macroscopic physical properties.

In geosciences, it typically is applied to the more difficult problem of which process(es) caused an observed pattern of preferred crystal orientation in rocks and aims at an interpretation of the kinematics and dynamics of geological processes including a consistent reconstruction of the geological deformation

history. The solution to this problem cannot be achieved by texture analysis only but requires a complete study of the microstructure and the entire geologic situation on different scales. Quantitative texture analysis in geosciences can but add an additional parameter to narrow down the multiple ambiguities of the geological problem. Therefore, this parameter itself should be conservatively estimated.

Although the typical metallurgical problems may be characterized as direct problems, the typical geoscientific problems are inverse problems.

The statistical distribution of orientations of crystal grains of the contributing phases within the specimen of a polycrystalline material is a simple mathematical approach to describe and quantify preferred crystal orientation; the orientation-density function is the basic entity of quantitative texture analysis. Employing more advanced statistics such as spatial correlation functions of crystal orientations would result in a sophisticated *orientation distribution analysis* in the sense of Sander's *axis distribution analysis* (Achsenverteilungsanalyse or AVA) (cf. Sander, 1934, 1948–50; Wenk and Trommsdorff, 1965; Braun, 1972).

However, even the basic orientation density function generally cannot be measured directly without destruction of the specimen. Furthermore, the measurement of individual crystal orientations is rather expensive in terms of either manpower of the human operator or automated equipment (cf. Schwarzer, 1991; Kunze and others, 1993; Adams, Wright, and Kunze, 1993). Therefore, it is usual practice to measure pole-density functions of several distinct reflections in X-ray or neutron diffraction experiments with a texture goniometer. Determining a reasonable orientation-density function from experimental pole-density functions then is the crucial prerequisite of quantitative texture analysis. Thus, at the center of the inverse geoscientific problem is an inverse mathematical problem.

This communication is concerned with the interpretation of orientation-density functions calculated from normal diffraction pole-density functions in general, and with the interpretation of orientation-density functions beyond the scope of quantitative texture analysis in metallurgy in particular. The general idea is that a geological orientation-density function should be a conservative estimate because it should provide an interpretation as safe (objective, unbiased, unprejudiced, honest, etc.) as possible given the pole-density function data. Thus, motivated by the objectives and purposes of quantitative texture analysis in geosciences mathematical methods and additional mathematical modeling assumptions should be applied which actually provide a conservative solution that allows safe interpretation, for example, in terms of the total number of recovered components of preferred orientation and their corresponding (integrated) density.

Geophysical Significance of Preferred Crystal Orientation

In order to interpret seismic data with some confidence it is necessary to know physical properties of these materials at pressures and temperatures at which they occur in the Earth's crust. They have to be measured in the laboratory. Among others, one topic of concern is the anisotropy of deformed rocks. Mylonites, deformed during ductile deformation, comprise large volumes of the Earth's crust and are expected to have anisotropic elastic properties. During ductile deformation minerals attain preferred orientation either by intracrystalline slip, by dynamic recrystallization, or by some other mechanism or a combination of all of them (Wenk, 1985).

Because component minerals are elastically anisotropic an aggregate with preferred orientation is also anisotropic. The relationship between texture and velocity anisotropy for instance has been established quantitatively for mantle peridotites and dunities (e.g., Crosson and Lin, 1971; Baker and Carter, 1972) and metals (e.g., Morris, 1969).

Implications of fault rocks and anisotropy on interpretation of seismic data include that travel times are not related by some simple function to distance (depth) but depend on the local geologic structure, and it is not clear which properties are responsible to produce a reflector surface. Compositional layering (e.g., Hale and Thompson, 1982), folding of layered structures, and anisotropy (e.g., Jones, 1985) have been suggested. Recently, Jones and Nur (1982, 1984) and Fountain, Hurich, and Smithson (1984) demonstrated that mylonite layers indeed can be seismic reflectors. Unless elastic properties are known for rocks composing the crustal segment of interest, interpretation of reflection seismic data is ambiguous.

This is where quantitative texture analysis may enter as it provides an additional way to characterize rocks. Systematic investigations may provide the answers to such questions of general geophysical interest as "is it possible to distinguish between cataclastic and ductile rocks from seismic properties?" or "can we distinguish compositional layering and anisotropy?" (Wenk, 1985). For a more detailed discussion of this topic, the reader is referred to Mainprice and Nicolas (1989).

THE INVERSION PROBLEM OF TEXTURE GONIOMETRY

In most applications one does not measure individual orientations but density distributions of particular lattice planes $(hkl) \in {}^{3}$ on continuous pole figures by diffraction experiments. Pole figures can be defined as graphical representations of the joint probability density function of normals to crystallographic lattice planes, that is, of poles. In order to obtain information about the orien-

tation distribution, it is necessary to deconvolute density information contained in measured pole figures. This process is termed "pole-figure inversion." It is done mathematically with various methods, and for that it is necessary to represent the orientation distribution by an orientation-density function $f(g)$. Depending on the method, the recovered orientation-density function $\hat{f}$ is continuous or a step function. Correspondingly, the pole distribution displayed in a pole figure is represented by a pole-density function. This inversion is not trivial, and some information about the orientation-density function cannot be retrieved without making additional mathematical modeling assumptions (Wenk and others, 1988).

Fundamental Projection Formula of Texture Goniometry

The unit sphere in ^{q} is denoted by S^{q-1}, q and $q-1$ indicate the topological dimension, respectively. [It should be noted that Müller (1966) and Watson (1983) use the notation $S^q \subset {}^{q}$.] Let $SO(3)$ denote the special orthogonal group of proper rotations g in ^{3}. The fundamental equation relating an orientation density function f defined on some set $G \subset SO(3)$ of orientations g and its corresponding pole density function $\tilde{P}_{\mathbf{h}}$ of the crystal form $\mathbf{h} = \{\mathbf{h}_m \mid m = 1, \ldots, M_{\mathbf{h}}\} \subset S^2$ defined for $\mathbf{r} \in S^3 \subset {}^{2}$ may be written as

$$\tilde{\mathcal{P}}_{\mathbf{h}}[f(g)](\mathbf{r}) = (\tilde{\mathcal{P}}_{\mathbf{h}} f)(\mathbf{r}) = C \int_G K(\mathbf{h}, \mathbf{r}; g) f(g) dv(g) = \tilde{P}_{\mathbf{h}}(\mathbf{r}) \qquad (1)$$

with $g \in G$ and $dv(g)$ the invariant Lebesgue volume element of the orientation space G, and with some normalization factor $C > 0$ such that

$$\int_{S^2_+} \tilde{P}_{\mathbf{h}}(\mathbf{r}) ds(\mathbf{r}) = 1$$

when

$$\int_G f(g) dv(g) = 1$$

where $ds(\mathbf{r})$ denotes the invariant Lebesgue surface element of $S^2 \subset {}^{3}$, and $S^2_+ = \{\mathbf{r} \in {}^{3} \mid \|\mathbf{r}\| = 1, r_3 \geq 0\}$ the upper unit sphere in ^{3} including its boundary. The distributional kernel $K(\mathbf{h}, \mathbf{r}; g)$ of the integral operator $\tilde{\mathcal{P}}_{\mathbf{h}}$ defined by Equation (1) may be written as

$$K(\mathbf{h}, \mathbf{r}; g) = \sum_{m=1}^{M_{\mathbf{h}}/2} [\delta(\mathbf{h}_m - g\mathbf{r}) + \delta(\mathbf{h}_m + g\mathbf{r})] \qquad (2)$$

with $\mathbf{h}_m \in S^2_+$, $m = 1, \ldots, M_{\mathbf{h}}/2$, where $M_{\mathbf{h}}$ denotes the multiplicity of the crystal form $\mathbf{h}$; for crystallographic terms the reader is refered to (Niggli, 1924, 1928).

By definition, Equation (1), $\tilde{P}_{\mathbf{h}}(\mathbf{r}) = \tilde{P}_{\mathbf{h}}(-\mathbf{r})$, that is a pole-density function of any crystal form is an even (antipodally symmetric) function regardless of the class of crystal symmetry. Thus, it may be thought of as a function defined on the upper (lower) unit hemisphere or equivalently on the two-dimensional projective plane (cf. Friedel, 1913; Laue, 1916, 1941).

Equation (2) may be read as K defining some one-dimensional lines $G_{\mathbf{h}_m}(\mathbf{r}) = \{g \in G | \mathbf{h}_m = g\mathbf{r}\}$, $m = 1, \ldots, M_{\mathbf{h}}$, of integration which in turn define the actual projection from G onto S^2_+. The integration paths are constituted of all proper rotations $g \in G$ mapping a given direction $\mathbf{r} \in S^2_+$ on one of the symmetrically equivalent directions $\mathbf{h}_m \in S^2_+$, $m = 1, \ldots, M_{\mathbf{h}}/2$, or $-\mathbf{h}_m \in S^2_+$, respectively

$$\tilde{P}_{\mathbf{h}}(\mathbf{r}) = \sum_{m=1}^{M_{\mathbf{h}}/2} (\tilde{\mathcal{P}}_{\mathbf{h}_m} f)(\mathbf{r}) = \sum_{m=1}^{M_{\mathbf{h}}/2} (\mathcal{P}_{\mathbf{h}_m} f + \mathcal{P}_{-\mathbf{h}_m} f)(\mathbf{r})$$

$$= C \sum_{m=1}^{M_{\mathbf{h}}} \int_{\{g \in G | \mathbf{h}_m = g\mathbf{r}\}} f(g) d\nu(g) = \Omega \sum_{m=1}^{M_{\mathbf{h}}} (\mathcal{P}_{\mathbf{h}_m} f)(\mathbf{r}) \qquad (3)$$

The set $\{g \in G | \mathbf{h}_m = g\mathbf{r}\}$ may be represented as the set of two successive rotations in terms of Euler angles. The first is a fixed rotation $g_1 = g_1(\varphi, \vartheta, 0)$ given in terms of the spherical coordinates (ϑ, φ), $\vartheta \in [0, \pi]$, $\varphi \in [0, 2\pi)$, of $\mathbf{r}$ mapping $\mathbf{r}$ onto $\mathbf{e}_3 = (0, 0, 1)$, and the second is a variable rotation $g_2^{-1} = g_2^{-1}(\alpha_m, \beta_m, \omega)$ given in terms of the spherical coordinates (β_m, α_m), $\beta_m \in [0, \pi]$, $\alpha_m \in [0, 2\pi)$, of $\mathbf{h}_m$ and a variable angle $\omega \in [0, 2\pi)$ mapping $\mathbf{e}_3$ onto $\mathbf{h}_m$ for all $\omega \in [0, 2\pi)$

$$\{g \in G | \mathbf{h}_m = g\mathbf{r}\} = \{g_2^{-1}(\alpha_m, \beta_m, \omega) g_1(\varphi, \vartheta, 0) | \omega \in [0, 2\pi)\} \qquad (4)$$

with

$$M(g_1) = \begin{pmatrix} \cos\varphi \cos\vartheta & \sin\varphi \cos\vartheta & -\sin\vartheta \\ -\sin\varphi & \cos\varphi & 0 \\ \cos\varphi \sin\vartheta & \sin\varphi \sin\vartheta & \cos\vartheta \end{pmatrix} \qquad (5)$$

and

$$M(g_2^{-1}) = M^t(g_2) =$$

$$\begin{pmatrix} \cos\alpha_m \cos\beta_m \cos\omega - \sin\alpha_m \sin\omega & -\cos\alpha_m \cos\beta_m \sin\omega - \sin\alpha_m \cos\omega & \cos\alpha_m \sin\beta_m \\ \sin\alpha_m \cos\beta_m \cos\omega + \cos\alpha_m \sin\omega & -\sin\alpha_m \cos\beta_m \sin\omega + \cos\alpha_m \cos\omega & \sin\alpha_m \sin\beta_m \\ -\sin\beta_m \cos\omega & \sin\beta_m \sin\omega & \cos\beta_m \end{pmatrix} \qquad (6)$$

Thus, switching to another notation

$$\tilde{P}(\beta, \alpha; \vartheta, \varphi) = C \sum_{m=1}^{M_h} \int_{(0, 2\pi)} f(g_2^{-1}(\alpha_m, \beta_m, \omega) g_1(\varphi, \vartheta, 0)) d\omega \qquad (7)$$

Therefore, pole-density functions may be read as some line integrals and its values may be interpreted as means along these lines in G. Equation (1) also may be characterized as Fredholm integral equation of first type.

The mathematical problem of quantitative texture analysis is to recover a reasonable approximate $\tilde{f}$ of f from experimental pole-density functions according to Equation (1). The quantities actually measured are defined by Equation (11).

Similar to this specific mathematical problem of texture goniometry, problems of mathematical tomography generally can be formulated as a Fredholm integral equation of the first type and were tackled conventionally by transform methods associated with Radon or Fourier type transforms or corresponding infinite series expansions (cf. Louis, 1989).

In texture analysis this approach has been pursued systematically by Bunge and coworkers (see Bunge, 1982) and received widespread acceptance; it is referred to as harmonic series expansion method. An orientation-density function calculated by the harmonic method generally is not nonnegative and generally exhibits local peaks representing components of preferred orientation which cannot be associated with crystal grains of the specimen and which do not correspond to its physical properties; these deviations from the (elusive) "true" orientation-density function were termed "ghosts" and are mathematical artifacts introduced by the method itself.

The explanation of "ghost" phenomena in orientation-density functions recovered with the harmonic method led to its major revision and a fundamental clarification of the mathematical texture problem (Matthies, 1982). Its major result may be summarized as follows. Because of the specifics of the normal diffraction experiment which cannot distinguish between the (mathematically distinct) upper and lower side of a crystallographic lattice plane, a pole-density function always is even implying that its odd Fourier coefficients with respect to spherical harmonics vanish. Therefore, the harmonic method basically is unable to recover the odd Fourier coefficients of the orientation-density function with respect to generalized spherical harmonics. The harmonic method is neither capable of applying the nonnegativity constraints on both pole-density functions and orientation-density function in a direct and constructive way but as a corrective device only.

The Indicator Approach to Pole-Density Function Inversion

Let $\mathcal{G}(N) = \{G_n | n = 1, \ldots, N\}$ be a partition of $G \subset SO(3)$ into volume elements of equal volume (for notational simplicity), and let

$$\chi_N^{(n)}(g) = 1_{G_n}(g) = \begin{cases} 1 & \text{if } g \in G_n \in \mathcal{G}(N) \\ 0 & \text{otherwise} \end{cases} \tag{8}$$

denote the indicator function with respect to $G_n \in \mathcal{G}(N)$. For every $N \in$ the set $\{\chi_N^{(n)}\}$ is an orthonormal total system of functions defined on G with respect to the weight function $\mathrm{vol}_3^{-1}(G_n)$, where $\mathrm{vol}_3(G_n)$ denotes the three-dimensional finite volume of $G_n \subset G$. Thus, every square integrable function $f \in \mathfrak{L}^2(G)$ can be approximated abitrarily by a linear combination of indicator functions. The set $\{\chi_N^{(n)}\}$ is closed. The analog is true for a partition $\mathcal{Z}(P) = \{Z_p | p = 1, \ldots, P\}$ of S_+^2 and corresponding indicator functions $1_{Z_p}(\mathbf{r})$ with respect to $\mathfrak{L}^2(S_+^2)$. The coefficients of the linear combination are referred to as Fourier coefficients with respect to indicators and weights, and the linear combination is referred to as Fourier orthogonal series expansion with respect to indicators.

The Fourier coefficients of an orientation-density function f with respect to the set of volume indicators now are defined as

$$x_n = \int_G f(g)\chi_N^{(n)}(g)dv(g) = \int_G f(g)1_{G_n}(g)dv(g)$$

$$= \int_{G_n} f(g)dv(g) \geq 0, \qquad n = 1, \ldots, N, N = 1, 2, \ldots \tag{9}$$

and $f \in \mathfrak{L}^2(SO(3))$ is associated with

$$f(g) \sim \lim_{N \to \infty} \sum_{n=1}^{N} x_n \chi_N^{(n)}(g)/\mathrm{vol}_3(G_n) \tag{10}$$

Analogously, the Fourier coefficients of a pole-density function $\tilde{P}_{\mathbf{h}}$ with respect to the set of surface indicators are defined as

$$y_p(\mathbf{h}) = \int_{Z_p} \tilde{P}_{\mathbf{h}}(\mathbf{r})ds(\mathbf{r}) \geq 0, \qquad p = 1, \ldots, P, P = 1, 2, \ldots \tag{11}$$

and $\tilde{P}_{\mathbf{h}}(\mathbf{r}) \in \mathfrak{L}^2(S^2)$ is associated with the infinite series

$$\tilde{P}_{\mathbf{h}}(\mathbf{r}) \sim \lim_{P \to \infty} \sum_{p=1}^{P} y_p(\mathbf{h})1_{Z_p}(\mathbf{r})/\mathrm{vol}_2(Z_p) \tag{12}$$

where $\mathrm{vol}_2(Z_p)$ denotes the two-dimensional finite volume of $Z_p \subset S_+^2$.

The Fourier coefficients have the obvious interpretation of $y_p(\mathbf{h})/\mathrm{vol}_2(Z_p)$ as mean diffracted intensity of the surface patch Z_p, $p = 1, \ldots, P$, and $\Sigma_{p=1}^{P} y_p = 1$; analogously $x_n/\mathrm{vol}_3(G_n)$ as mean orientation density of the orientation box G_n, $n = 1, \ldots, N$, and $\Sigma_{n=1}^{N} x_n = 1$.

Practical applications are confined to the partial sums

$$\hat{f}(g) = \sum_{n=1}^{N} x_n \chi_N^{(n)}(g)/\mathrm{vol}_3(G_n) \tag{13}$$

$$\hat{\tilde{P}}_{\mathbf{h}}(\mathbf{r}) = \sum_{p=1}^{P} y_p(\mathbf{h}) 1_{Z_p}(\mathbf{r})/\mathrm{vol}_2(Z_p) \tag{14}$$

with sufficiently large N and P, respectively.

Indicator Orientation Ghosts

Indicator functions which only can take on the values 0 or 1 are neither even nor odd. Let $\mathbf{h} \in Z_{p_2} \in \mathcal{Z}(P)$ be fixed; applying the projection $\mathcal{P}_{\mathbf{h}}$ to $1_{G_{n_0}}$ with $g_{n_0} \in G_{n_0}$ such that $g_{n_0}\mathbf{r} = \mathbf{h}$ for some $\mathbf{r} \in Z_{p_1} \in \mathcal{Z}(P)$ yields

$$\mathcal{P}_{\mathbf{h}}[1_{G_{n_0}}(g)](\mathbf{r}) \neq 1_{Z_{p_1}}(\mathbf{h}) 1_{Z_{p_1}}(\mathbf{r}) \tag{15}$$

That is, the indicator $1_{G_{n_0}}$ of the orientation box G_{n_0} containing an orientation g_{n_0} rotating $\mathbf{r} \in Z_{p_1} \subset S^2$ into $\mathbf{h} \in Z_{p_2} \subset S^2$ generally is not projected by $\mathcal{P}_{\mathbf{h}}$ onto the indicator $1_{Z_{p_1}}$ of the surface patch Z_{p_1} of an arbitrary partition $\mathcal{Z}(P)$, that is, canonical partitions do not seem to exist.

Nevertheless, the pole-density functions corresponding to the indicators $\chi_N^{(n)}$ of the orientation boxes G_n are defined as

$$\begin{aligned} \tilde{E}_{\mathbf{h}}^{n(N)}(\mathbf{r}) &= (\tilde{\mathcal{P}}_{\mathbf{h}}\chi_N^{(n)})(\mathbf{r}) \\ &= \sum_{m=1}^{M_{\mathbf{h}}/2} \int_G \{\delta(\mathbf{h}_m - g\mathbf{r}) + \delta(\mathbf{h}_m + g\mathbf{r})\}\chi_N^{(n)}(g)d\nu(g) \not\equiv 0 \qquad (16) \\ &\qquad (n = 1, \ldots, N) \end{aligned}$$

which have been termed "elementary pole figures" by Ruer (1976). These elementary pole-density functions $\tilde{E}_{\mathbf{h}}^{n(N)}$ do not provide a mathematically well-behaved system of functions defined on S^2 or S_+^2, respectively, because they are neither orthogonal nor linearly independent.

The latter should become plausible by the following argument. Let the crystal form $\mathbf{h}$ have symmetrically equivalent constituents $\mathbf{h}_1, \ldots, \mathbf{h}_{M(\mathbf{h})}$ ordered such that $\mathbf{h}_{m+i} = -\mathbf{h}_i$, $i = 1, \ldots, m$, $m = M(\mathbf{h})/2$. Now let $g_1 \in G_{n_1} \in \mathcal{G}(N)$ such that $g_1\mathbf{h}_i = \mathbf{r}_i$, $g_1\mathbf{h}_{m+i} = -\mathbf{r}_i$, $i = 1, \ldots, m$. Then an orientation $g_2 \notin G_{n_1}$ exists with $g_2\mathbf{h}_i = -\mathbf{r}_{\alpha(i)}$, $i = 1, \ldots, m$, for some permutation σ of the set $\{1, \ldots, m\}$, and $g_2\{\mathbf{h}\} = g_1\{\mathbf{h}\}$. Hence, $\tilde{E}_{\mathbf{h}}^{n_2(N)} \sim \tilde{E}_{\mathbf{h}}^{n_1(N)}$ (cf. Schaeben, 1984).

Then, with Equation (1) and (16)

$$\begin{aligned} (\tilde{\mathcal{P}}_{\mathbf{h}}\hat{f})(\mathbf{r}) &= \tilde{\mathcal{P}}_{\mathbf{h}}\left[\sum_{n=1}^{N} x_n\chi_N^{(n)}(g)/\mathrm{vol}_3(G_n)\right](\mathbf{r}) \\ &= \sum_{n=1}^{N} x_n\tilde{E}_{\mathbf{h}}^{n(N)}(\mathbf{r})/\mathrm{vol}_3(G_n) \end{aligned} \tag{17}$$

From this argument it should be plausible that the $x_n \geq 0$ are not determined uniquely by Equation (17), but that at least $N/2$ can be selected arbitrarily provided $x_n \geq 0$ ($n = 1, \ldots, N$). In contrast to the harmonic analysis it now is no longer obvious which of the unknowns x_n to select as free parameters. Thus, it does not make sense to say that the undeterminable portion of an orientation-density function cannot be represented by indicators; the implication of the harmonic series expansion to split an orientation-density function into an even uniquely determined and an odd undeterminable portion no longer seems to be reasonable. Using indicators, an undeterminable portion, which makes (non)sense by its own, does not exist. The representation and apparition of ghost orientations depends on the representation of an orientation-density function itself.

Comparing Equation (14) and (17) leads to the system of linear equations

$$y_p(\mathbf{h}) = \sum_{n=1}^{N} \pi_{pn}(\mathbf{h}) x_n, \qquad p = 1, \ldots, P \tag{18}$$

with matrix elements $\pi_{pn}(\mathbf{h})$, $p = 1, \ldots, P$, $n = 1, \ldots, N$, defined by

$$\pi_{pn}(\mathbf{h}) = C \int_{Z_p} \int_{G_n} \sum_{m=1}^{M_{\mathbf{h}}} 1_{G_{\mathbf{h}_m(\mathbf{r})}}(g) dv(g) ds(\mathbf{r}) \tag{19}$$

and constraints

$$0 \leq x_n \leq 1, \qquad n = 1, \ldots, N \tag{20}$$

and

$$\sum_{n=1}^{N} x_n = 1 \tag{21}$$

It should be noted that the elementary pole figures $\tilde{E}_{\mathbf{h}}^{n(N)}$ are the column vectors of the matrix $\pi_{PN}(\mathbf{h})$. Equation (18) reads in matrix notation

$$\pi(\mathbf{h})\mathbf{x} = \mathbf{y}(\mathbf{h}) \tag{22}$$

Subject to constraints (20) and (21), Equation (22) is the fundamental projection equation of texture goniometry in terms of Fourier coefficients with respect to indicators.

The matrix $\pi(\mathbf{h})$ is large, sparse, column-rank deficient, and without structure, the augmented matrix $(\pi(\mathbf{h}), \mathbf{y}(\mathbf{h}))$ may be inconsistent. It requires additional mathematical modeling assumptions to uniquely specify a particular solution. They usually are formulated as an optimization problem with an appropriate objective function. The candidate favored here is the entropy functional

$$S(x_1, \ldots, x_N) = -\sum_{n=1}^{N} x_n \ln x_n \tag{23}$$

Variation Width of Feasible Orientation-Density Functions

Adapting the continuous notation of Equation (1), the variation width of all feasible orientation density functions is defined by

$$0 \le l(g) \le f(g) \le u(g),\ g \in G \tag{24}$$

as

$$V_q(f; \mathfrak{F}) = \left\{ \frac{1}{\mathrm{vol}_3(G)} \int_G |u(g) - l(g)|^q d\nu(g) \right\}^{1/q}, \qquad q \in \tag{25}$$

with $l(g)$, $u(g)$ defined pointwise for each $g \in G$ by

$$l(g) = \inf_{f \in \mathfrak{F}} f(g), \qquad g \in G \tag{26}$$

$$u(g) = \sup_{f \in \mathfrak{F}} f(g), \qquad g \in G \tag{27}$$

where $\mathfrak{F}$ denotes the set of all feasible orientation-density functions with respect to a given set of experimental pole-density functions $\tilde{P}_{\mathbf{h}}$ of crystal forms $\mathbf{h}$. It should be noted that the functions $l(g)$ and $u(g)$ are not probability density functions, and hence not orientation-density functions. Furthermore, it is emphasized that they depend on the available set of pole-density functions.

In the notation of indicators [Eq. (22)] of Equation (1) the data dependent variation width of feasible orientation-density functions is defined by

$$0 \le l_n \le x_n \le u_n, \qquad n = 1, \ldots, N \tag{28}$$

as

$$V_q(\mathbf{x}; \mathcal{Z}(P), \mathcal{G}(N), \mathfrak{F}) = \left\{ \sum_{n=1}^{N} |u_n - l_n|^q \right\}^{1/q}, \qquad q \in \tag{29}$$

with $\mathbf{l}, \mathbf{u} \in$ ^{N} given by the sequence of $2N$ optimization problems

$$\min F_n = \min \mathbf{e}_n\mathbf{x} = l_n, \text{ resp. } \max F_n = \max \mathbf{e}_n\mathbf{x} = u_n,$$
$$n = 1, \ldots, N \tag{30}$$

subject to

$$\pi(\mathbf{h})\mathbf{x} = \mathbf{y}(\mathbf{h}), \qquad x_n \ge 0, \qquad n = 1, \ldots, N,$$
$$\sum_{n=1}^{N} x_n = 1 \tag{31}$$

where $\mathbf{e}_n$ denotes the nth unit vector of ^{N}.

It is emphasized that the bounds **l** and **u** depend on the given set of pole-density functions and the discretization, that is on the partitions $\mathcal{Z}(P)$ of the hemisphere $S^2_+ \subset$ ^{3} of poles, and $\mathcal{G}(N)$ of the orientation space $G \subset SO(3)$.

Each individual optimization problem of the sequence (30) is a problem of linear programming (LP) with an extremely simple linear objective function.

Maximum Entropy Solution of Pole-Density Inversion with Indicators

The maximum entropy solution may be addressed as the feasible orientation-density function, which is most uniform with respect to entropy, that is which is most conservative with the least content of information consistent with the available pole density function data. The actual solution is achieved by the maximum entropy preferred orientation portion in the sense of (23), and constraints (20), (21), and (22), and maximum uniform portion.

The maximum entropy solution is also the most safely balanced solution in the sense of the Backus–Gilbert formalism (Backus and Gilbert, 1967, 1968, 1970; Parker, 1977; Kirsch, Schomburg, and Berendt, 1988), that is it delivers the best resolution given the partitions (G_n) of G and (Z_p) of S^2_+.

The corresponding optimization problems may be solved by general purpose large-scale mathematical programming algorithms involving the simplex method, a quasi Newton method, the reduced-gradient method, and a projected Lagrangian method or by a special purpose algorithm (Lent, 1976; Lent and Censor, 1989; Schaeben, 1988, 1991).

This special purpose algorithm supplemented by additionally incorporating a simple minimum density adjustment reads

$$x_m^{(0)} = \begin{cases} 0 & \text{if } \pi_{pm}(\mathbf{h}) \neq 0 \text{ and } y_p = 0 \\ \dfrac{1}{N - \nu} & \text{otherwise} \end{cases} \qquad m = 1, \ldots, N \quad (32)$$

where ν denotes the number of a priori zero components of $\mathbf{x}^{(0)}$,

$$x_m^{(k+1)} = \prod_{p \in L_m(\mathbf{h})} \left\{ \left(\frac{y_p(\mathbf{h})}{\sum_{n=1}^{N} \pi_{pn}(\mathbf{h}) \bar{x}_n^{(k)}} \right)^{\rho_k \pi_{pm}(\mathbf{h})} \right\} \max(x_m^{(k)}, b)$$

$$m = 1, \ldots, N \quad (33)$$

with $L_m(\mathbf{h}) = \{p \mid \pi_{pm}(\mathbf{h}) \neq 0\}$ denoting the set of numbers referring to the nonzero elements of the mth column vector of $\pi(\mathbf{h})$, and relaxation parameters $0 < \rho_k \leq 1$, and

$$\bar{x}^{(k)} = \sum_{l<m} x_l^{(k+1)} \mathbf{e}_l + \sum_{l \geq m} x_l^{(k)} \mathbf{e}_l \quad (34)$$

b usually is selected to be the smallest normalized measured intensity $y_{\min}$.

This augmented algorithm does not provide the maximum entropy solution of the inversion problem, but the maximum entropy solution conditional to the heuristic maximum uniform portion adjustment.

It applies immediately to complete or incomplete pole density functions as well as to simultaneous processing of several pole-density functions of different crystal forms **h**. The necessary nonnegativity of the orientation-density function to be recovered is a truly constitutive element, possible zero components in the pole-density function are exactly and efficiently accounted for, uniform pole-density functions give a uniform orientation-density function. Furthermore, it is numerically stable and straightforward.

CASE STUDY OF A QUARTZ TEXTURE

Resolution of Coincidences

In geoscientific applications of quantitative texture analysis, such as a complete fabric analysis in terms of crystallographic orientations rather than crystallographic axes, another difficulty may arise which here is exemplified for quartz. Because of coincidences or partial superpositions of peaks in the diffraction diagram, that is the result of identical or experimentally undistinguishable Bragg angles, only superposed pole-density functions can be measured with the goniometer. In the situation of quartz and for $l \neq 0$ and $h \neq k$, only the superposed $(hkil) + (khil)$ − pole-density functions can be experimentally determined. If their relative weighs β_i are known, different crystal forms with indentical distances of crystal lattice planes are taken into account by

$$\left[\sum_{i=1}^{s} \beta_i \pi(\mathbf{h}^{(i)})\right] \mathbf{x} = \sum_{i=1}^{s} \beta_i \mathbf{y}(\mathbf{h}^{(i)}) = \mathbf{y}(\mathbf{h}^*) \tag{35}$$

with $\Sigma_{i=1}^{s} \beta_i = 1$. The $k + 1$st iteration of the generalized algorithm (33) then reads

$$\begin{aligned} x_m^{(k+1)} &= \prod_{p \in L_m} \left\{ \left[\frac{y_p(\mathbf{h})}{y_p^{(k)}(\mathbf{h}^*)} \right]^{r_k \Sigma_{i=1}^{s} \beta_i \pi_{pm}(\mathbf{h}^{(i)})} \right\} \max(x_m^{(k)}, y_{\min}) \\ &= \prod_{i=1}^{s} \prod_{p \in L_m} \left\{ \left[\frac{y_p(\mathbf{h}^*)}{y_p^{(k)}(\mathbf{h}^*)} \right]^{r_k \beta_i \pi_{pm}(\mathbf{h}^{(i)})} \right\} \max(x_m^{(k)}, y_{\min}) \end{aligned} \tag{36}$$

with $y^{(k)}(\mathbf{h}^*) = [\Sigma_{i=1}^{s} \beta_i \pi(\mathbf{h}^{(i)})]\, \bar{\mathbf{x}}^{(k)}$.

From (36) it is obvious that the $\pi(\mathbf{h}^*)$ matrix $\Sigma_{i=1}^{s} \beta_i \pi(\mathbf{h}^{(i)})$ corresponding to the superposed pole-density functions need not be calculated but that another geometric mean with respect to the weighs β_i will do. The geometric mean stems from the definition (23) of entropy and the concept of maximum entropy.

Practical Application and Results

Quartzite fabrics (Fig. 1) are of considerable interest in structural geology because they should aid in a consistent reconstruction of the deformation history which generated the observed pattern of preferred orientation, that is, in identifying and interpreting the deformation mechanisms, the shape of the finite strain ellipsoid, and the strain path or kinematic framework (cf. Schmid and Casey, 1986).

Analysis and interpretation of the complete fabric in terms of crystal orientations, that is in terms of the distribution of the major crystal forms, is accomplished by the interpretation of a conservative estimate of the orientation-density function determined from normal diffraction pole-density functions. For quartz usually the pole-density functions of the crystal forms $a(110)$, $m(100)$, and of the superposition of the forms $r(101)$ and $z(011)$ weighed by their structure factors 0.7 and 0.3, respectively, are measured incompletely in the range of 0 to roughly 80 degrees polar angle. From these data the program MENTEX (Maximum ENtropy TEXture) written in major parts by the first author and jointly developed into a comprehensive package for quantitative texture analysis by the authors calculates the orientation-density function with maximum entropy subject to maximum uniform portion. With this orientation-density function it then is possible to recalculate and complete incomplete experimental pole-density functions, to calculate additional pole-density functions, for example, of crystal forms such as $c(001)$ which cannot be measured by X-ray diffraction at all, or the resolved pole-density functions of the forms $r(101)$ and $z(011)$ which cannot be measured individually.

For the following example experimental pole-figure data of the (110), (100),

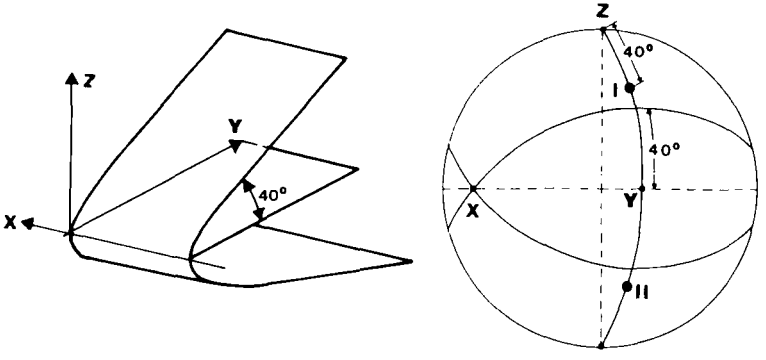

Figure 1. Idealized sketch of fold geometry of quartzite sample DO282. Z = direction of principal compressive stress, X = direction of principal tensile stress, = direction of principal extension, = fold axis, = extension lineation, XY = plane of flattening.

and 0.3 * (011) + 0.7 * (101) quartz reflections up to 80 degrees polar angle (Fig. 2A–2C) were provided by Thomas Dortmann to demonstrate features of the MENTEX program system and to check earlier interpretations (Dortmann, 1987). The sample DO282 was taken from a quartzite fold in the Sesia-Lanzo

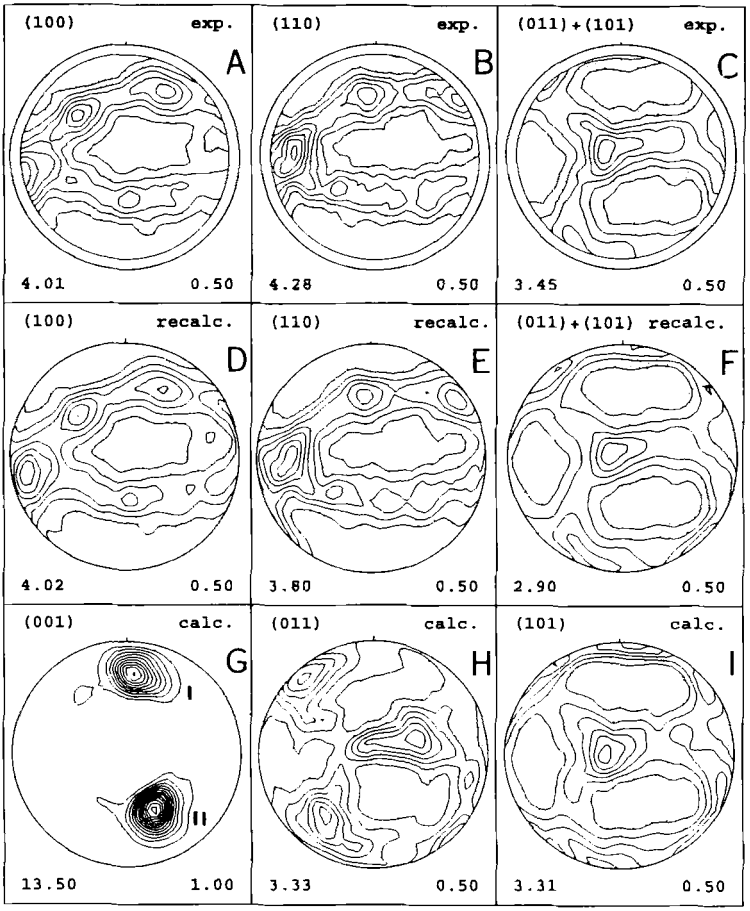

Figure 2. Experimental and (re)calculated quartz pole figures of sample DO282 in equal area projection; dotted area below 1.0 times uniform; lower left: maximum density; lower right: contour interval. A, B, C: Experimental quartz pole figures. D, E, F: Recalculated pole figures from the MENTEX orientation density function after 23 iterations with A, B, C as input pole figures. G, H, I: Calculated pole figures from the MENTEX orientation density function after 23 iterations with A, B, C as input pole figures.

Zone, Val Sesia, Northern Italy. The interpretation of optical and X-ray measurements is cited briefly here (Dortmann, 1987; translation by these authors): "In the crest of the fold there is on each limb a schistosity plane. They are both oriented approximately 40 degrees to the flattening plane (*XY*). The *c*-axis diagram [measured optically] shows two maxima with approximately the same density and both are oriented 40 degrees to the axis of compressive stress (*Z*) in the plane *ZY*. The *a*-axes [(110) measured by X-ray diffraction] are distributed on two great circles which are both approximately 40 degrees inclined to the flattening plane. One single strong *a*-axis maximum is located near the direction of principal extension (*X*) in the point of the intersection of the two great circles. The prism *m*-planes [(100) measured by X-ray diffraction] reveal the same great circle pattern as the *a*-axes. In the course of increasing flattening the two *c*-axis maxima rotate toward the axis of compression (*Z*) and the schistosity planes as well as the great circles rotate into the plane of flattening (*XY*). Therefore, the strain symmetry in the crest of the fold is orthorhombic. The preferred orientation of the *c*-axes and the common *a*-axes maximum in the extension direction indicate *a*-slip in the basal-plane as major slip system."

The incomplete experimental pole figures (Fig. 2A–2C) measured with a Philips X'PERT goniometer with ATC-3 texture supplement were used to calculate the orientation distribution with maximum entropy preferred orientation portion and maximum uniform portion, and, in turn, to recalculate the complete pole figures (Fig. 2D–2F); it took 23 steps of iterations of the procedure (33) and (36), respectively, until the stopping criteria concerning the increase of entropy and the decrease of deviation of input and recalculated pole-figure data were satisfied. The recalculated pole figures are in good agreement with the experimental pole figures. The (011) + (101) pole figure has been resolved into its two constituent parts (Fig. 2H, 2I) and the (001) pole figure has been calculated (Fig. 2E). This pole figure shows two distinct maxima at an azimuth of 85 degrees and polar angle of 60 degrees (maximum I, density 10 times uniform) and at an azimuth of 295 degrees and polar angle of 47 degrees (maximum II, density 13.5 times uniform). These maxima represent the poles of two fiber axes. The (100) and (110) pole figures reveal two great circle distributions with some local maxima within these patterns. This interpretation is confirmed by inspecting the orientation-density function. Several sections of the orientation-density function are shown in Figure 3. There are two tubes of high density pervading the orientation space parallel to the φ_2-axis, tube I with a mean density of about 10 and tube II with a mean density of about 16 times uniform. The tubes show some local maximum densities above the corresponding mean densities, for example, for $\varphi_1 = 295$, $\Phi = 47$, $\varphi_2 = 15$ with a density of 32. All identified mayor texture components are listed in Table 1.

These texture components have been used to define a mathematical model

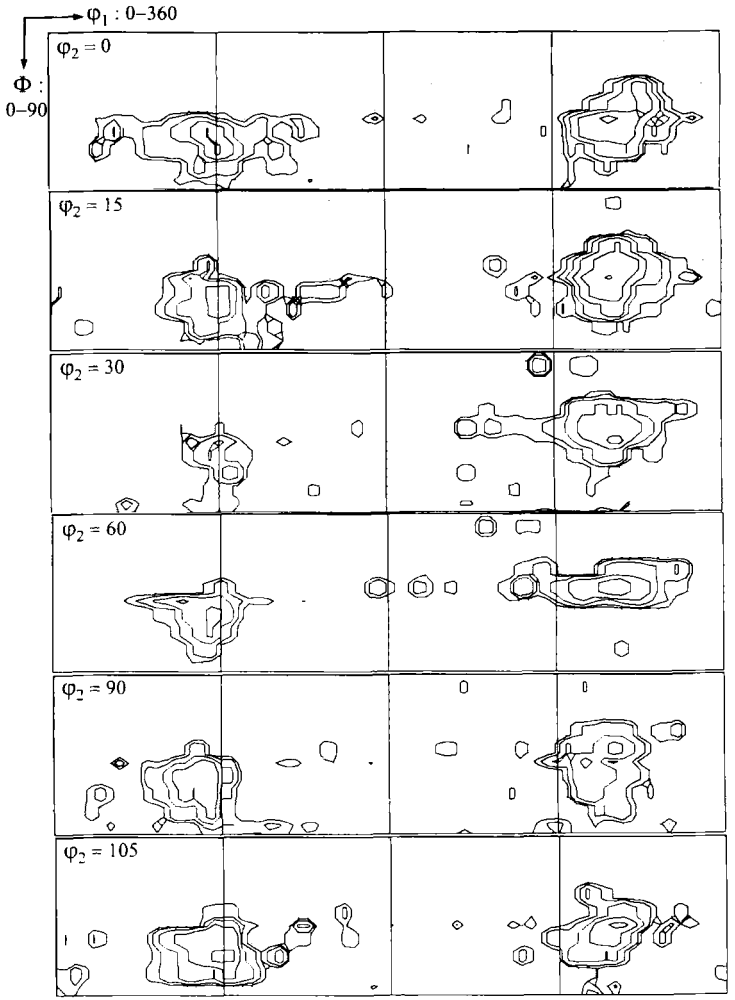

Figure 3. MENTEX orientation-density function calculated from (110), (100), and (011) + (101) incomplete pole figures with 23 iterations; contours 1, 2, 4, 8, 16, 32 times uniform.

Table 1. Components of Quartz Texture

	Position of the components			Mathematical model odf[a]	
	Azimuth angle	Pole angle	Rotation around the pole	Gaussian portion	Standard odf[a] half width
I fiber axis (001)					
fiber	85	60		16.0 %	27
maximum	85	60	5	10.0 %	27
maximum	85	60	75	8.5 %	27
maximum	85	60	100	8.5 %	27
II fiber axis (001)					
fiber	295	47		33.0 %	27
maximum	295	47	15	20.0 %	27
uniform portion				4 %	

[a]For standard orientation distributions (see Matthies, Vinel, and Helming, 1987).

orientation-density function (Matthies, Vinel, and Helming, 1987) composed of Gauss-shaped distributions with the listed parameters (Table 1). Figure 4 displays the same sections of the orientation space as plotted in Figure 3. The maximum densities and the position of the maxima along the tubes are similar in both orientation-density functions, but the mathematical model provides a simplified approximate and represents only the most prominent features of the calculated MENTEX distribution.

Direct modeling of experimental pole figure data with texture components could be performed by a "component fit" method introduced by Helming and Eschner (1990) and may result in an exhaustive recognition of texture components.

The corresponding mathematical model pole figures are presented in Figure 5A–5C and Figure 5G, 5H; they excellently exhibit the essential features of the experimental and calculated pole figures of Figure 2. In order to demonstrate the reliability of the MENTEX procedure the (011) + (101) pole figure has been recalculated once in 6 iterations using the mathematical model pole figures of the reflections (100), (110), and (011) + (101) (Fig. 5F), and then also in five iterations from the (100), (110), (011), and (101) pole figures (Fig. 5I). Both calculated (011) + (101) pole figures cannot be distinguished.

In order to analyze the *a*-axis and *m*-prism maxima in *X* (extension axis) the major components of the texture have been plotted separately in Figure 6 for the (110) reflection and in Figure 7 for the (100) reflection. All components

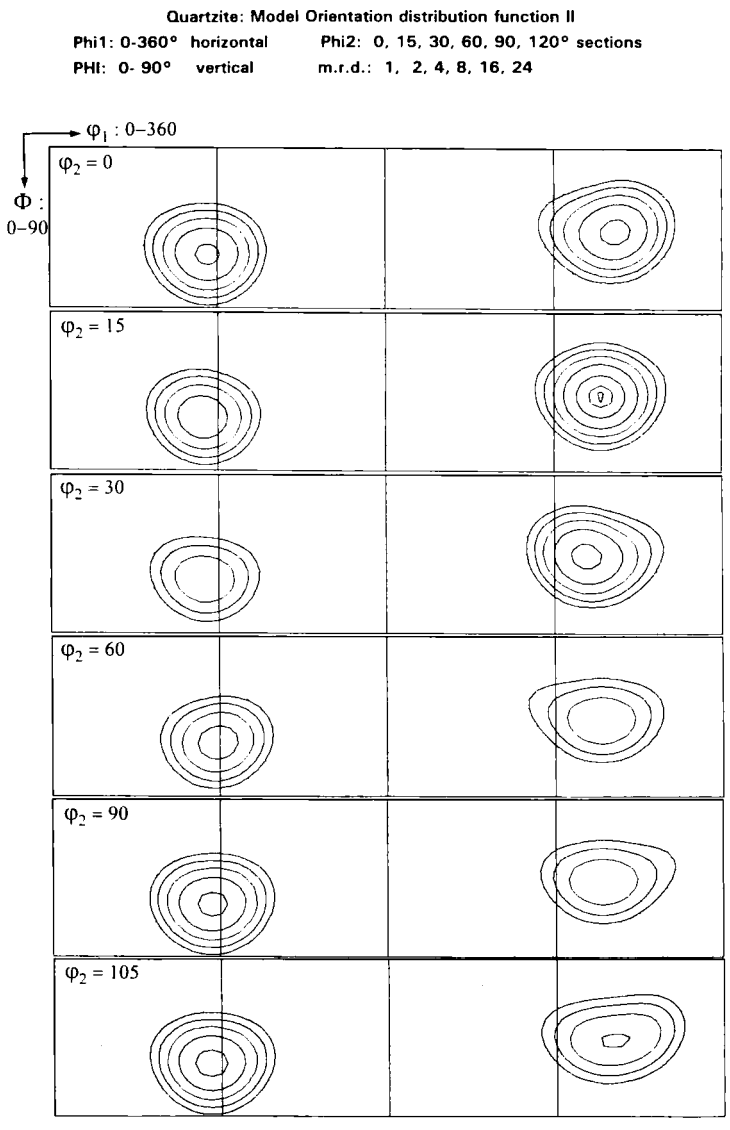

Figure 4. Mathematical model orientation-density function composed of Gaussian distributions according to Table 1; contours 1, 2, 4, 8, 16, 32 times uniform.

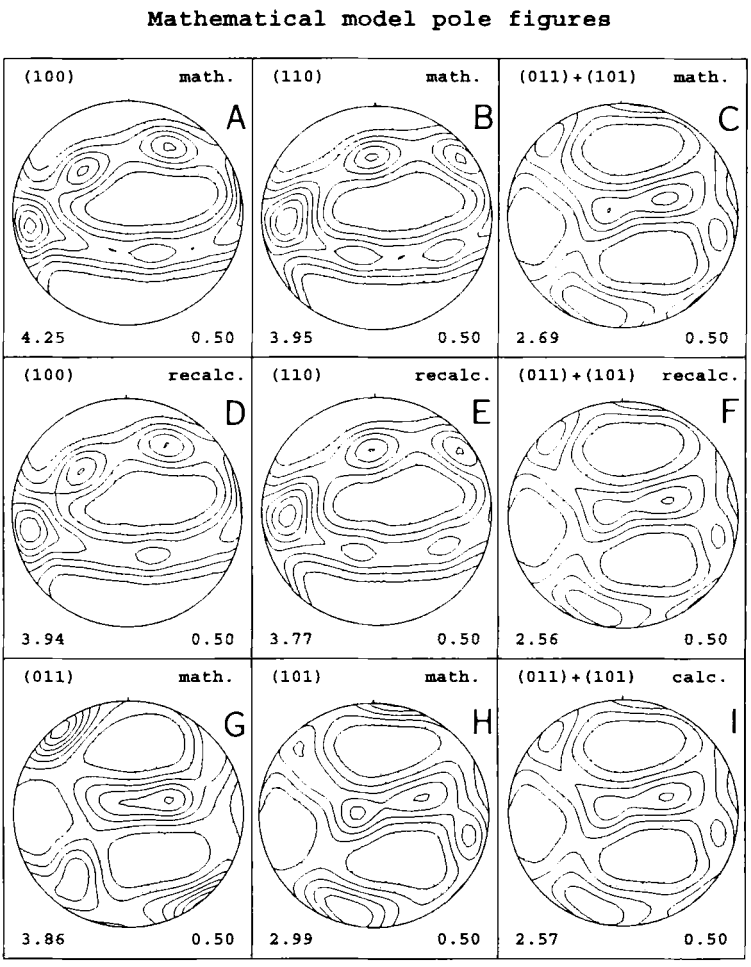

Figure 5. Corresponding mathematical model and (re)calculated pole figures. A, B, C: Mathematical model pole figures. D, E, F: Recalculated pole figures from the MENTEX orientation density function after six iterations with A, B, C as input pole figures. G, H: Mathematical pole figures, I: Calculated pole figure from the MENTEX orientation density function after 5 iterations with A, B, G, H as input pole figures.

contribute to the *a*-axis maximum in *X* but only the two rather weak components (85,60,5) and (85,60,75) are exactly centered on *X* (Fig. 6C, 6D), that is the maximum is not owed just to the superposition of the two great circle distributions. The same holds for the *m*-prism, but here the strong components

Components of the mathematical model pole figures

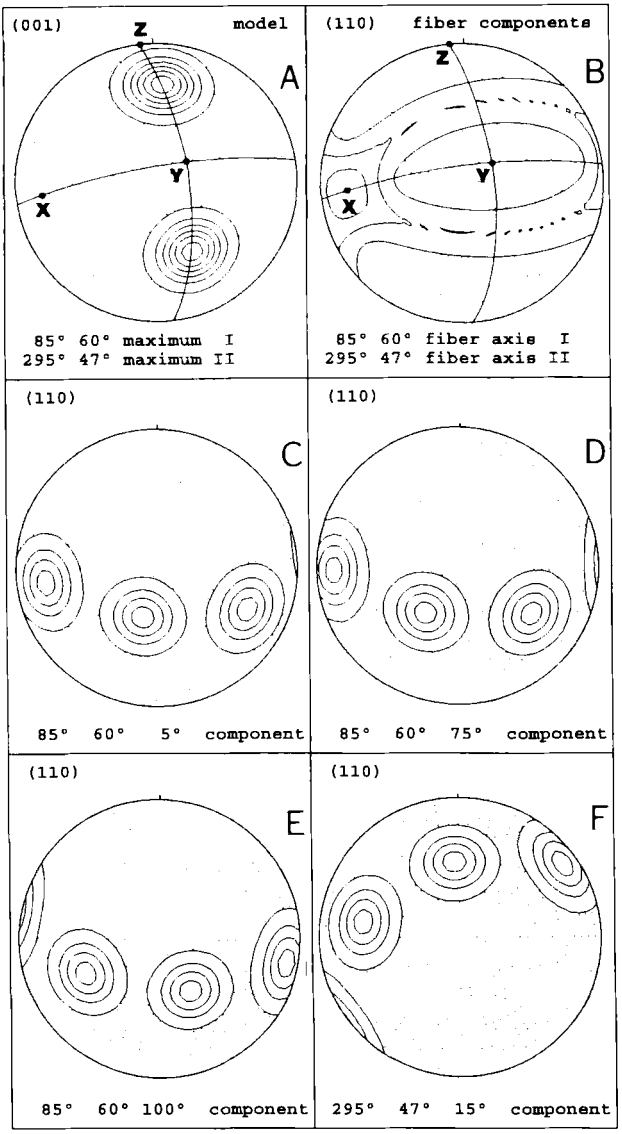

Figure 6. Major texture components texture for (110) reflection. A: c-axes maximum I, II, B: corresponding a-axes fibers I, II, C: component (86,60,5) within fiber I centered on X, D: component (85,60,75) within fiber I centered on X, E: component (85,60,100) within fiber I, F: component (295,47,15) within fiber II.

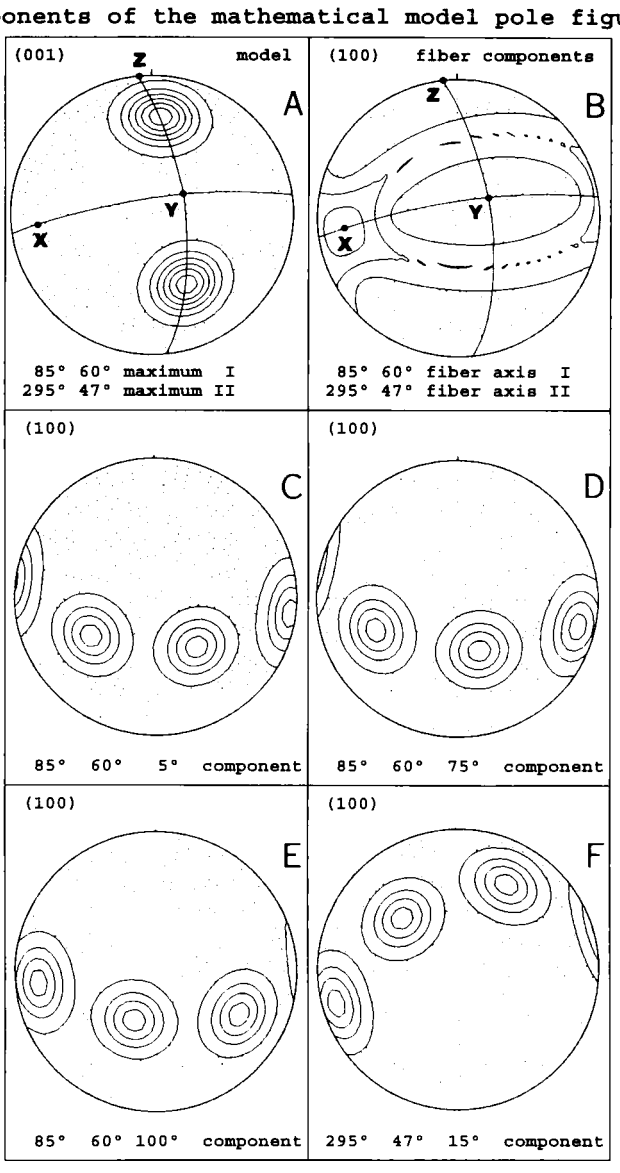

Figure 7. Major texture components texture for (100) reflection. A: *c*-axes maximum I, II, B: corresponding *m*-prism fibers I, II, C: component (85,60,5) within fiber I, D: component (85,60,75) within fiber I, E: component (85,60,100) within fiber I close to *X*, F: component (295,47,15) within fiber II close to *X*.

(85,60,100) and (295,47,15) are located only close to X (Fig. 7E, 7F). Thus Dortmann's (1987) conclusion is confirmed that basal a-slip may have contributed preferentially to the deformation process but other systems must have been operating, too; otherwise one probably would expect that all components are centered with (110) on X.

CONCLUSIONS

The solution of the tomographic inversion problem of texture goniometry presented here employs series expansion into indicator functions, entropy optimization, and is given by an algorithm that allows efficient programming. Thus, it relates explicitly to a well-established body of mathematical and information theory and liberates the user from confidence in *ad hoc* procedures. Practical application requires only incompletely measured pole figures of a few reflections which may be coincident, and is straightforward. The calculated MENTEX orientation-density function always is nonnegative, and provides a conservatively estimated orientation-density function supporting an interpretation that is safe and detailed in terms of components of preferred orientation.

As the case study of a quartz texture demonstrates, a visually appealing representation and first interpretation of preferred crystal orientation is facilitated by reference to numerically completed pole figures that initially were measured incompletely, and additionally to calculated pole figures that actually were not measured or cannot be measured at all with X-ray diffraction. Both numerical operations require an orientation distribution. However, understanding of preferred crystal orientation is increased only by explicit reference to an orientation distribution, that is, by a close inspection of the calculated orientation-density function and a consistent analysis of its components.

Thus, the maximum entropy texture method incorporated in the package MENTEX is well suited to geoscientific applications of texture analysis where comparison of observed patterns with a few well understood standard patterns corresponding to metallurgical processes is insufficient.

ACKNOWLEDGMENTS

It is acknowledged gratefully that Thomas Dortmann kindly provided the data set DO282 of experimental pole-figure data measured with a Philips X'PERT goniometer with ATC-3 texture supplement. The authors would like to thank Brent L. Adams, Brigham Young University, Provo, and Ute C. Herzfeld, University of Colorado, Boulder, for their careful review of the manuscript.

REFERENCES

Aczel, J., and Daroczy, Z., 1975, On measures of information and their characterizations: Academic Press, New York, 234 p.

Adams, B. L., Wright, S. I., and Kunze, K., 1993, Orientation imaging: the emergence of a new microscopy: Metall. Trans. A, in press.

Aki, K., and Richards, P. G., 1980, Quantitative seismology, theory and methods: W. H. Freeman & Comp., San Francisco, 432 p.

Artzy, E., Elfving, T., and Herman, G. T., 1979, Quadratic optimization for image reconstruction II: Comp. Graphics Image Proc., 11, p. 242-261.

Backus, G. E., and Gilbert, J. F., 1967, Numerical applications of a formalism for geophysical inverse problems: Geophys. Jour. Roy. Astr. Soc., v. 13, no. 1-3, p. 247-276.

Backus, G. E., and Gilbert, J. F., 1968, The resolving power of gross earth data: Geophys. Jour. Roy. Astr. Soc., v. 16, no. 2, p. 169-205.

Backus, G. E., and Gilbert, J. F., 1970, Uniqueness in the inversion of inaccurate gross earth data: Phil. Trans. Roy. Soc., Ser. A, v. 266, no. 1173, p. 123-192.

Baker, D. W., and Carter, N. L., 1972, Seismic velocity anisotropy calculated for ultramafic minerals and aggregates, *in* Heard, H. C., Borg, I. Y., Carter, N. L., Raleigh, C. B., eds., Flow and fracture of rock—The Griggs Volume: Am. Geophys. Union, Geophysical Monograph 16, p. 157-166.

Blum, E. K., 1972, Numerical analysis and computation—theory and praxis: Addision & Wesley Publ. Co., Reading, Massachusetts, 612 p.

Braun, G., 1972, Computerdarstellung von Achsenverteilungsanalysen: Geol. Rdschau., v. 61, no. 3, p. 849-871.

Bunge, H. J., 1969, Mathematische Methoden der Texturanalyse: Akademie Verlag, Berlin, 330 p.

Bunge, H. J. (P. R. Morris trans.), 1982, Texture analysis in materials science: Butterworths, London, 593 p.

Burg, J. P., 1967, Maximum entropy spectral analysis: Proc. 37th Meeting Soc. Exploration Geophysicists (reprinted in Childers, D. G., ed., 1978, Modern spectrum analysis: John Wiley & Sons, New York, p. 34-41.

Burg, J. P., 1975, Maximum entropy spectral analysis: unpubl. doctoral dissertation, Stanford University, 136 p.

Censor, Y., 1982, Entropy optimization via entropy projections, *in* Drenick, W. R. F., and Kozin, F., eds., System modeling and optimization: Springer Verlag, Berlin, p. 450-454.

Censor, Y., 1983, Finite series—expansion reconstruction methods: Proc. IEEE, v. 71, no. 3, p. 409-419.

Censor, Y., and Segman, J., 1987, On block-iterative entropy maximization: Jour. Information and Optimization Sciences, v. 8, no. 3, p. 275-291.

Crosson, R. S., and Lin, J. W., 1971, Voigt and Reuss prediction of anisotropic elasticity of dunite: Jour. Geophys. Res., v. 76, no. 2, p. 570-578.

Dortmann, T., 1987, Gesteine, Strukturen und Metamorphose am Alpensüdrand: Die Sesia-Lanzo-Zone im Val Sesia, Norditalien: unpubl. doctoral dissertation, Univ. Köln, 143 p.

Edward, J. A., and Fitelson, M. M., 1973, Notes on maximum-entropy processing: IEEE Trans. Inform. Theory, IT 19, 232-234.

Fountain, D. M., Hurich, C. A., and Smithson, S. B., 1984, Seismic reflectivity of mylonite zones in the crust: Geology, v. 12, no. 4, p. 195-198.

Friedel, G., 1913, Sur les symetries cristallines que peut reveler la diffraction des rayons Röntgen: C. R. Acad. Sci., Paris, v. 157, no. 26, p. 1533-1536.

Frieden, B. R., 1980, Statistical models for the image restoration problem: Comput. Graphics Image Processing, v. 12, no. 1, p. 40–59.

Gibbs, J. W., 1875–78, On the equilibrium of heterogeneous substances: Connecticut Acad. Arts and Science Trans., v. 3, p. 108–248, 343–524 (reprinted 1928, Longmans, Green & Co, New York; 1961, Dover Publications, New York, 2 v.).

Hale, L. D., and Thompson, G. A., 1982, The seismic reflection character of the Mohorovičić discontinuity: Jour. Geophys. Res., v. 87, no. 6, p. 4625–4635.

Helming, K., and Eschner, T., 1990, A new approach to texture analysis of multiphase materials using a texture component model: Cryst. Res. Technol., v. 25, no. 8, p. K203–K208.

Herman, G. T., 1982, Mathematical optimization versus practical performance. A case study based on the maximum entropy criterion in image reconstruction: Math. Programming Studies, v. 20, p. 96–112.

Herman, G. T., 1985, Application of maximum entropy and Bayesian optimization methods to image reconstruction from projections, *in* Smith, C. R., and Grandy, W. T. Jr., eds., Maximum entropy and Bayesian methods in inverse problems: D. Reidel Publ. Company, Dordrecht, p. 319–338.

Jaynes, E. T., 1957a, Information theory and statistical mechanics: Phys. Rev., v. 106, p. 620–630.

Jaynes, E. T., 1957b, Information theory and statistical mechanics II: Phys. Rev., v. 108, p. 171–190.

Jaynes, E. T., 1968, Prior probabilities: IEEE Trans. Syst. Sci. Cybern, SSC 4, no. 3, p. 227–241.

Jaynes, E. T., 1979, Where do we stand on maximum entropy?, *in* Levine, R. D., Tribus, M., eds., The maximum entropy formalism, MIT Press, Cambridge, Massachusetts, p. 15–118.

Jaynes, E. T., 1982, On the rationale of maximum-entropy methods: Proc. IEEE, v. 70, no. 9, p. 939–952.

Jaynes, E. T., 1983, Papers on probability, statistics, and statistical physics: D. Reidel Publ. Co., Dordrecht, 434 p.

Jaynes, E. T., 1985, Where do we go from here?, *in* Smith, C. R., and Grandy, W. T. Jr., eds., Maximum entropy and Bayesian methods in inverse problems: D. Reidel Publ. Co., Dordrecht, p. 21–58.

Jones, T. D., 1985, Nature of seismic reflections from the crystalline basement—COCORP Wind River Line, Wyoming: Jour. Geophys. Res., v. 90, no. 8, p. 6783–6791.

Jones, T. D., and Nur, A., 1982, Seismic velocity and anisotropy in mylonites and the reflectivity of deep crustal faults: Geology, v. 10, no. 5, p. 260–263.

Jones, T. D., and Nur, A., 1984, The nature of seismic reflections from deep crustal fault zones: Jour. Geophys. Res., v. 89, no. 5, p. 3153–3171.

Kapur, J. N., 1983, Twenty-five years of maximum-entropy methods: Jour. Math. Phys. Sci., v. 17, no. 2, p. 103–156.

Katz, A., 1967, Principles of statistical mechanics—the information theory approach: Freeman, San Francisco, 188 p.

Khinchin, A. I., 1957, Mathematical foundations of information theory: Dover Publications, New York, 120 p.

Kirsch, A., Schomburg, B., and Berendt, G., 1988, The Backus-Gilbert method: Inverse Prob., v. 4, no. 3, p. 771–783.

Kullback, S., 1959, Information theory and statistics: John Wiley & Sons, New York, 395 p.

Kunze, K., Wright, S. I., Adams, B. L., and Dingley, D. J., 1993, Advances in automatic EBSP single orientation measurements: Textures and Microstructures, in press.

Laue, M. von, 1916, Über die Symmetrie der Kristall—Röntgenogramme: Ann. Physik, IV. Folge, Bd 50, p. 433–446.

Laue, M. von, 1941, Röntgenstrahlinterferenzen: Physik und Chemie und ihre Anwendungen in Einzeldarstellungen, Bd. VI, Akademische Verlagsgesellschaft Becker & Erler Kom.-Ges., Leipzig, 367 p.

Lent, A., 1976, A convergent algorithm for maximum entropy image restoration, with a medical X-ray application, *in* Shaw, R., ed., Image Analysis and Evaluation: Society of Photographic Scientists and Engineers, Washington DC, p. 249–257.

Lent, A., and Censor, Y., 1989, The primal-dual algorithm as a constraint-set-manipulation device: Mathematical Programming, preprint, 33 p.

Louis, A. K., 1989, Inverse und schlecht gestellte Probleme: Teubner, Stuttgart, 205 p.

Mainprice, D., and Nicolas, A., 1989, Development of shape and lattice preferred orientations—application to the seismic anisotropy of the lower crust: Jour. Structural Geology, 11, no. 1–2, p. 175–189.

Matthies, S., 1982, Aktuelle Probleme der quantitativen Texturanalyse: Akademie der Wissenschaften der DDR, Zentralinstitut für Kernforschung, Rossendorf bei Dresden, ZfK-480, 211 p.

Matthies, S., Vinel, G. W., and Helming, K., 1987, Standard distributions in texture analysis, vol. 1: Akademie Verlag, Berlin, 442 p.

McLaughlin, D. W., ed., 1983, Inverse problems: Proc. Applied Mathematics: Am. Math. Soc., Providence, Rhode Island, 189 p.

Menke, W., 1984, Geophysical data analysis: Discrete inverse theory: Academic Press, Orlando, 260 p.

Morris, P. R., 1969, Averaging fourth-rank tensors with weight functions: Jour. Appl. Phys., v. 40, p. 447–448.

Müller, C., 1966, Spherical harmonics: Springer-Verlag, Berlin, 45 p.

Niggli, P., 1924, Lehrbuch der Mineralogie (2nd ed.): Verlag von Gebrüder Borntraeger, Berlin, 712 p.

Niggli, P., 1928, Krystallographische und strukturtheoretische Grundbegriffe, *in* Wien, W., and Harms, F., eds., Handbuch der Experimentalphysik, Band 7, 1. Teil, Akademische Verlagsgesellschaft mbH, Leipzig, 317 p.

Parker, R. L., 1977, Understanding inverse theory: Ann. Rev. Earth Planet Sci., v. 5, p. 35–64.

Rietsch, E., 1977, The maximum entropy approach to inverse problems: Jour. Geophys., v. 42, no. 5, p. 489–506.

Rowlinson, J. S., 1970, Probability, information and entropy: Nature, v. 225, no. 5239, p. 1196–1198.

Ruer, D., 1976, Methode vectorielle d'analyse de la texture: unpubl. masters thesis, Metz, 163 p.

Sander, B., 1934, Fortschritte der Gefügekunde der Gesteine, Anwendungen, Ergebnisse, Kritik: Fortschr. Mineral. Petrgr., v. 18, p. 111–170.

Sander, B., 1948–50, Einführung in die Gefügekunde der geologischen Körper, vol. 2: Springer-Verlag, Vienna, v. 1, 215 p.; v. 2, 409 p.

Schaeben, H., 1984, Mathematical modeling of the orientation distribution function by the vector method of quantitative texture analysis: Physica, Status Solidi B, v. 123, no. 2, p. 425–434.

Schaeben, H., 1988, Entropy optimization in quantitative texture analysis: Jour. Appl. Phys., v. 64, no. 4, p. 2236–2237.

Schaeben, H., 1991, Entropy optimization in quantitative texture analysis: II. Application to pole-to-orientation density inversion: Jour. Appl. Phys., v. 69, no. 3, p. 1320–1329.

Schmid, S. M., and Casey, M., 1986, Complete fabric analysis of some commonly observed quartz c-axis patterns, *in* Hobbs, B. E., and Heard, H. C., eds., Mineral and rock deformation: laboratory studies—The Paterson Volume: Geophysical Monograph 36, Am. Geophys. Union, p. 263–286.

Schwarzer, R. A., 1991, Crystal texture analysis by means of electron diffraction, *in* Bunge, H. J.,

and Esling, C., eds., Advances and applications of quantitative texture analysis: DGM Informationsgesellschaft Verlag, Oberursel, p. 51–72.

Shannon, C. E., 1948, A mathematical theory of communication: Bell System Tech. Jour., v. 27, p. 379–423, 623–656.

Shannon, C. E., and Weaver, W., 1949, The mathematical theory of communication: Univ. Illinois Press, Urbana, 117 p.

Shaw, R., ed., 1976, Image analysis and evaluation: Soc. Photographic Scientists and Engineers (Washington, D.C.), 538 p.

Smith, C. R., and Grandy, W. T. Jr., eds., 1985, Maximum entropy and bayesian methods in inverse problems: D. Reidel Publ. Co., Dordrecht, 492 p.

Tarantola, A., 1987, Inverse problem theory: Elsevier, Amsterdam, 613 p.

Tikhonov, A. N., and Arsenin, V. Y., 1977, Solutions of ill-posed problems: Halstead Press, New York, 258 p.

Titterington, D. M., 1985, Common structure of smoothing techniques in statistics: Internat. Statist. Rev., v. 53, p. 141–170.

Tolman, R. C., 1938, Principles of statistical mechanics: Oxford Univ. Press, London, 660 p.

Tribus, M., 1961, Thermostatistics and thermodynamics: Van Nostrand, Princeton, 649 p.

Tribus, M., 1979, Thirty years of information theory, *in* Levine, R. D., and Tribus, M., eds., The maximum entropy formalism: MIT Press, Cambridge, Massachusetts, p. 1–14.

Watson, G. S., 1983, Statistics on spheres: John Wiley & Sons, New York, 238 p.

Wenk, H. R., ed., 1985, Preferred orientation in deformed metals and rocks. An introduction to modern texture analysis: Academic Press, Orlando, 610 p.

Wenk, H. R., and Trommsdorff, V., 1965, Koordinatentransformation, mittelbare Orientierung, Nachbarwinkelstatistik. Gefügekundliche Rechenprogramme mit Beispielen: Beitr. Min. Petr., v. 11, no. 6, p. 559–585.

Wenk, H. R., Bunge, H. J., Kallend, J. S., Lücke, K., Matthies, S., Pospiech, J., and Van Houtte, P., 1988, Orientation distributions: Representation and determination, *in* Kallend, J. S., and Gottstein, G., eds., Proc. ICOTOM8 (Santa, Fe, New Mexico) The Metallurgical Society, p. 17–30.

APPENDIX. THE RATIONALE OF THE MAXIMUM ENTROPY CONCEPT

Essential to this method is the term "entropy" and its meaning in information theory. It is well known in thermodynamics (Gibbs, 1875–78; Tribus 1961), in statistical mechanics (Jaynes, 1957a, 1957b; Katz, 1967; Tolman, 1938), and in information theory (Aczel and Daroczy, 1975; Khinchin, 1957; Kullback, 1959; Shannon, 1948; Shannon and Weaver, 1949). Initially different definitions of the term have been unified and the entropy concept has comprehensively been discussed by Jaynes (1979, 1982, 1985), Kapur (1983), Tribus (1979). In fact, the concept of entropy optimization revitalized and rehabilitated the concept of Bayes' *a priori* probabilities (Jaynes, 1968).

The entropy of a discrete random variable Z, respectively of its discrete probability distribution, is defined formally as

$$S_n(Z) = S(p_1, \ldots, p_n) = -\sum_{j=1}^{n} p_j \ln p_j \geq 0 \qquad (37)$$

Thus, entropy provides a measure of the "lack of information" or "uncertainty" inherent in a distribution when adapting a probabilistic view as opposed to a deterministic view.

Elementary Linkage of Probability and Information

The information content with respect to a possible result of an experiment which probes the ensemble ("draw a ball from the urn") depends on the distribution function: in the situation of a uniform distribution the lack of knowledge is complete, and each possible result of an experiment is equally likely (probable); in a well-pronounced unimodal distribution the lack of knowledge is relaxed, some results are more likely (probable) than others. If this distribution degenerates to Dirac's δ-distribution, the knowledge is almost complete and one is back in the almost-deterministic world.

Now, let the discrete probabilities be thought of as unknowns given by constraints in form of a system of linear equations $A\mathbf{p} = \mathbf{q}$ with some given $(m \times n)$ matrix A and some experimentally given values q_i, $i = 1, \ldots, m$. If the matrix A is of full rank, the system has the unique solution $\mathbf{p} = A^{-1}\mathbf{q}$ and the information of this distribution quantified by its entropy may be calculated immediately. If the matrix is of rank deficiency, the system has several different solutions, in fact infinitely many, of which a specific one may be selected by an additional mathematical model assumption. Thus, the solution with maximum entropy is the one with minimum information content consistent with the given data; thus it avoids artifacts and does not pretend a resolution for which there is no evidence in the data.

Combinatorial Reasoning

The next combinatorial argument is the result of Jaynes (1982) and Frieden (1980). Let L elements of luminance be distributed over n pixels to form a scene, the jth pixel receiving a portion of $p_j = L_j/L$, $j = 1, \ldots, n$, of the total luminance. Out of the total number n^L of conceivable outcomes of this random experiment, the number of outcomes which yield a particular set of frequencies $p_1, \ldots, p_n$ is

$$W(p_1, \ldots, p_n) = \frac{L!}{(p_1 L)!, \ldots, (p_n L)!} \tag{38}$$

Taking the limit for increasingly large L, and using Stirling's approximate yields

$$\lim_{L \to \infty} \frac{1}{L} \ln W(p_1, \ldots, p_n) = S(p_1, \ldots, p_n) \tag{39}$$

Thus, it may be argued that the probability law that could have existed in the maximum number of ways may well be presumed also to be the most likely one to have existed (Frieden, 1980).

Jaynes' Concentration theorem

This argument was developed further into the concentration theorem by Jaynes (1982). Let $\mathcal{C}$ be the subclass of all possible outcomes that could be observed in L trials of the random experiment as described, compatible with $m < n$ linearly indepenent constraints of the form

$$\sum_{j=1}^{n} a_{ij}p_j = q_i, \qquad j = 1, \ldots, m \tag{40}$$

Then a certain fraction F of the outcomes in class $\mathcal{C}$ will yield an entropy in the range of

$$S_{\max} - \Delta S \leq S(p_1, \ldots, p_l) \leq S_{\max} \tag{41}$$

The functional relation connecting F and ΔS is given by the concentration theorem that asymptotically

$$2L\Delta S \sim \chi^2_{I-J-1} \tag{42}$$

(Jaynes, 1982) where χ^2_{I-J-1} denotes the χ^2-distribution with $I - J - 1$ degrees of freedom.

Thus, it is concluded that the feasible distributions are concentrated strongly near the one of maximum entropy.

Constrained Maximum Entropy

If there are no other constraints imposed on the p_j than

$$0 \leq p_j \leq 1, \qquad j = 1, \ldots, n \tag{43}$$

and

$$\sum_{j=1}^{n} p_j = 1 \tag{44}$$

then maximizing $S(p_1, \ldots, p_n)$ results in the uniform distribution $p_j = 1/n$, $j = 1, \ldots, n$, and its maximum entropy $S_{\max}(1/n, \ldots, 1/n) = \ln n$.

Now let the probability distribution (p_j) be subject to m linear constraints of the form

$$\sum_{j=1}^{n} a_{ij}p_j = q_i, \qquad i = 1, \ldots, m \tag{45}$$

or in matrix notation

$$A\mathbf{p} = \mathbf{q} \tag{46}$$

If the system Equation (46) has a unique solution, it is given by $p = A^{-1}q$ and its entropy can be calculated according to Equation (37). If A is rank

deficient, the particular solution with maximum entropy is selected from the set of all solutions. This leads to a problem of constrained optimization

$$S(p_1, \ldots, p_n) = -\sum_{j=1}^{n} p_n \ln p_n = \max \tag{47}$$

subject to

$$A\mathbf{p} = \mathbf{q}, \qquad 0 \le p_j \le 1, \qquad j = 1, \ldots, n, \sum_{j=1}^{n} p_j = 1 \tag{48}$$

Taking the classic Lagrangian approach or the Kuhn–Tucker conditions (cf. Blum, 1972) for a constrained extremum towards the corresponding dual problem the unique solution is obtained

$$p_j = \frac{1}{Z(\lambda)} \exp\left(-(A^t\lambda)_j\right) = \frac{1}{Z(\lambda)} \exp\left(-\sum_{i=1}^{m} \lambda_i a_{ij}\right), \qquad j = 1, \ldots, n \tag{49}$$

with the partition function

$$Z(\lambda) = Z(\lambda_1, \ldots, \lambda_m) = \sum_{j=1}^{n} \exp\left(-\sum_{i=1}^{m} \lambda_i a_{ij}\right) \tag{50}$$

where the Lagrangian multipliers λ_i are given by

$$-\frac{\partial}{\partial \lambda_i} \ln Z(\lambda) = q_i, \qquad i = 1, \ldots, m \tag{51}$$

respectively by

$$\sum_{j=1}^{n} a_{ij} \exp(-A^t\lambda)_j) = q_i, \qquad i = 1, \ldots, m \tag{52}$$

resulting in the maximum entropy

$$S_{\max} = \ln Z(\lambda) + \sum_{i=1}^{m} \lambda_i q_i \tag{53}$$

(cf. Kapur, 1983; Jaynes, 1985). It should be noted that the solution is of exponential form, Equation (49), resulting from the definition of entropy [Eq. (37)]. From a computational point of view formulae (49) to (53) do not look too attractive because of their exponential and logarithmic terms.

This model is equivalent to the method of regularization (Tikhonov and Arsenin, 1977; Titterington, 1985) when the penalty term is selected to be the entropy functional (Jaynes, 1983; McLaughlin, 1983).

Fortunately, there is a computationally more appealing alternative. Ap-

proaching the primal problem results in a problem of convex programming, and solving both the primal and dual problem simultaneously results in an iterative procedure. Under the mathematically mild assumptions that

(i) $0 \leq a_{ij} \leq 1$,

(ii) A has no zero rows,

(iii) $A\mathbf{p} = \mathbf{q}$ has a nonnegative solution, and

(iv) there is a real number $c > 0$ such that $A\mathbf{p}^* = \mathbf{q}$ implies $\Sigma_{j=1}^{n} p_j^* = c$

the sequence

$$p_j^{(0)} = \begin{cases} 0 & \text{if } a_{ij} \neq 0 \text{ and } q_i = 0 \\ \dfrac{1}{n - \nu} & \text{otherwise} \end{cases} \tag{54}$$

where ν denotes the number of *a priori* zero components of $\mathbf{p}^{(0)}$, and

$$p_j^{(k+1)} = \left(\frac{q_{i_k}}{q_{i_k}^{(k)}}\right)^{\rho_k a_{i_k j}} p_j^{(k)} = \left(\frac{q_{i_k}}{\Sigma_{l=1}^{n} a_{i_k l} \bar{p}_l^{(k)}}\right)^{\rho_k a_{i_k j}} p_j^{(k)} \tag{55}$$

with cyclic control $i_k = k \pmod m + 1$, relaxational parameters $0 < \rho_k \leq 1$, and $\bar{p}_l^{(k)} = p_l^{(k+1)}$ if $l < k$ or $\bar{p}_l^{(k)} = p_l^{(k)}$ if $l \geq k$, converges toward the maximum entropy solution of system Equation (46), that is, it provides the solution of the constrained optimization problem Equation (47) subject to Equation (48).

This solution has been characterized as the particular one which all other solutions of the system Equation (46) are concentrated around in Jaynes "concentration theorem" (Jaynes, 1979, 1985).

Equation (55) may be rewritten in blockwise notation as

$$p_j^{(k+1)} = \prod_{i \in L_j} \left\{ \left(\frac{q_i}{q_i^{(k)}}\right)^{\rho_k a_{i_k j}} \right\} p_j^{(k)} \tag{56}$$

with $L_j = \{i \mid a_{ij} > 0\}$ grouping all components q_i of $\mathbf{q}$ which are related to p_j via nonzero matrix-elements a_{ij}.

The sequence defined by Equation (56) was labeled "block-iterative" algorithm (Censor and Segman, 1987). Proofs of convergence of this type of algorithms towards the maximum entropy solution of problem (47) subject to (48) have been given (Censor and Segman, 1987; Lent, 1976; Artzy, Elfving, and Herman, 1979; Censor, 1983; Lent and Censor, 1989).

If the system of equations, Equation (45) has to be replaced by some system of inequalities resulting from large errors in the measurements,

$$-\epsilon_i \leq q_i - \sum_{j=1}^{n} a_{ij} p_j \leq \epsilon_i, \qquad i = 1, \ldots, m \tag{57}$$

then a generalized algorithm (Censor, 1982) applies

$$p_j^{(0)} = \begin{cases} 0 & \text{for all } j \text{ for which } a_{ij} \neq 0 \text{ and } q_i = 0 \\ \dfrac{1}{N - \nu} & \text{otherwise} \end{cases} \tag{58}$$

where ν denotes the number of a priori zero components of $\mathbf{p}^{(0)}$, and

$$\mathbf{u}^{(0)} = \mathbf{0} \in \quad ^P \tag{59}$$

$$p_j^{(k+1)} = p_j^{(k)} \exp(c^{(k)} a_{i_k j}) \tag{60}$$

$$\mathbf{u}^{(k+1)} = \mathbf{u}^{(k)} - c^{(k)} \mathbf{t}_{p_k} \tag{61}$$

with $\mathbf{t}_{p_k} = \mathbf{e}_{p_k} \in IR^P$ and where $c^{(k)} = \text{mid}\{u_{p_k}^{(k)}, \delta^{(k)}, \delta_+^{(k)}\}$ with $\delta^{(k)}$, resp. $\delta_+^{(k)}$, given by

$$\sum_{j=1}^{n} a_{i_k j} p_j^{(k)} \exp(\delta_+^{(k)} a_{i_k j}) = q_{i_k} - \epsilon_{i_k} \tag{62}$$

and

$$\sum_{j=1}^{n} a_{i_k j} p_j^{(k)} \exp(\delta_-^{(k)} a_{i_k j}) = q_{i_k} + \epsilon_{i_k} \tag{63}$$

Notes and Remarks

For reasons of completeness it should be mentioned that about 20 years ago the maximum entropy method was introduced into exploration geophysics by Burg (1967, 1975) to model a solution of an estimating problem in spectral analysis and revolutionized geophysical spectrum analysis (cf. Edward and Fitelson, 1973; Rietsch, 1977). Today it is treated in any modern textbook of geophysics, for example, Aki and Richards (1980), Menke (1984), Smith and Grandy (1985), and Tarantola (1987). Smith and Grandy (1985) is entirely dedicated to this subject. For its use in computer tomography and image reconstruction the reader is referred particularly to Herman (1982, 1985) and Shaw (1976).